© 2016. Published by The Company of Biologists Ltd | Development (2016) 143, 3522-3531 doi:10.1242/dev.132936

RESEARCH ARTICLE

Vinculin b deficiency causes epicardial hyperplasia and coronary vessel disorganization in zebrafish

Feng Cheng[1,2], Liyun Miao[1,2], Qing Wu[3], Xia Gong[1], Jingwei Xiong[3,*] and Jian Zhang[1,*]

ABSTRACT

Coronary vessel development is a highly coordinated process during heart formation. Abnormal development and dysfunction of the coronary network are contributory factors in the majority of heart disease. Understanding the molecular mechanisms that regulate coronary vessel formation is crucial for preventing and treating the disease. We report a zebrafish gene-trap *vinculin b* (*vclb*) mutant that displays abnormal coronary vessel development among multiple cardiac defects. The mutant shows overproliferation of epicardium-derived cells and disorganization of coronary vessels, and they eventually die off at juvenile stages. Mechanistically, Vclb deficiency results in the release of another cytoskeletal protein, paxillin, from the Vclb complex and the upregulation of ERK and FAK phosphorylation in epicardium and endocardium, causing disorganization of endothelial cells and pericytes during coronary vessel development. By contrast, cardiac muscle development is relatively normal, probably owing to redundancy with Vcla, a vinculin paralog that is expressed in the myocardium but not epicardium. Together, our results reveal a previously unappreciated function of vinculin in epicardium and endocardium and reinforce the notion that well-balanced FAK activity is essential for coronary vessel development.

KEY WORDS: Vinculin, Coronary vessel, Epicardium, Cytoskeleton, Zebrafish

INTRODUCTION

The bulk of the vertebrate heart consists of cardiomyocytes and fibroblasts. In addition, the heart contains endothelial cells, which constitute the endocardium and coronary vessels, and epicardial cells. Heart development is a highly coordinated sequential process that includes heart field induction, cardiac cell migration, heart tube formation, cardiac looping, chamber specification and maturation, and coronary vessel formation (Harrison et al., 2015; Staudt and Stainier, 2012). Towards the end of cardiac development, the newly formed coronary vessels supply oxygen and nutrients to the inner cardiomyocytes, a process that is essential for survival (Harrison et al., 2015; Reese et al., 2002). Coronary diseases are a leading cause of death in industrialized countries, and understanding the development and physiology of coronary vessels is crucial in their prevention and treatment. Coronary vessel development is proposed to involve both vasculogenesis and angiogenesis (Munoz-Chapuli et al., 2002; Olivey et al., 2004). Previous studies in mouse and chicken showed that precursors of coronary vessels derive from the sinus venous, endocardium and epicardium (Dettman et al., 1998; Red-Horse et al., 2010; Vrancken Peeters et al., 1999; Wu et al., 2012). A recent report demonstrated that coronary vessels originate from endocardium-derived arterial cells by angiogenic sprouting, and identified Cxcr4a-Cxcl12b as a key signaling axis for this process in zebrafish (Harrison et al., 2015). However, the molecular mechanisms that regulate coronary vessel formation and patterning are still not well understood.

Formation of the complex coronary network requires highly coordinated cell-to-cell and cell-to-extracellular matrix (ECM) interactions, in which the cytoskeleton is essential for the transduction of cell force and of extracellular signals into cells. The cytoskeletal protein vinculin is localized in the integrin-mediated cell-ECM adhesions and cadherin-mediated cell-cell junctions (Geiger, 1979; Lifschitz-Mercer et al., 1997; Raz and Geiger, 1982). Vinculin mediates force transmission from cell matrix to actin cytoskeleton by interacting with other cytoskeletal proteins, such as talin, actinin and β-catenin (Zamir and Geiger, 2001; Ziegler et al., 2006). In addition, vinculin integrates extracellular signals essential for cellular survival and processes including differentiation, apoptosis and locomotion (Carisey and Ballestrem, 2011). Coordination of these processes is crucial for embryonic development and tissue homeostasis. The human vinculin (*VCL*) gene contains 22 exons (Moiseyeva et al., 1993). Exon 19 can be alternatively spliced, resulting in two protein isoforms: VCL and metaVCL (Koteliansky et al., 1992). VCL is ubiquitously expressed, whereas metaVCL, the larger isoform containing an additional 68 amino acid residues from exon 19, is expressed exclusively in cardiac and smooth muscle (Belkin et al., 1988). Mutations in *VCL* have been identified in human dilated cardiomyopathy (DCM) patients (Olson et al., 2002). In mice, vinculin (*Vcl*) gene deletion is lethal during gestation, with abnormal neural tube formation and cardiac defects (Xu et al., 1998a). However, mice with a cardiomyocyte-specific deletion of *Vcl* survive to adulthood. In the first 3 months, the mutant mice show 50% mortality and those that do survive longer exhibit dilated cardiomyopathy (Zemljic-Harpf et al., 2007). These results suggest that vinculin exerts important functions in cells other than cardiomyocytes. It remains incompletely understood how vinculin regulates heart development and function.

Another protein involved in cardiovascular development is focal adhesion kinase (FAK). FAK is ubiquitously expressed and is involved in cell survival and motility by mediating integrin, growth factor, and mechanical stress signaling (Mitra et al., 2005; Parsons, 2003). FAK is highly expressed in the developing vasculature (Polte et al., 1994). Consistently, *Fak* (*Ptk2*) null mouse embryos die at E8.5 with multiple defects, including a disorganized cardiovascular

[1]State Key Laboratory of Molecular Developmental Biology, Institute of Genetics and Developmental Biology, Chinese Academy of Sciences, Beijing 100101, China. [2]University of Chinese Academy of Sciences, Beijing 100049, China. [3]Institute of Molecular Medicine, Beijing Key Laboratory of Cardiometabolic Molecular Medicine and State Key Laboratory of Natural and Biomimetic Drugs, Peking University, Beijing 100871, China.

*Authors for correspondence (jingwei_xiong@pku.edu.cn; jianzhang84@genetics.ac.cn)

J.Z., 0000-0002-5867-9808

Received 12 November 2015; Accepted 26 July 2016

Development (2016) 143, 3522-3531 doi:10.1242/dev.132936

system (Ilić et al., 1995). FAK controls cell survival and the motility of endothelial cells and smooth muscle cells during angiogenesis (Braren et al., 2006; Hauck et al., 2000; Peng et al., 2004; Shen et al., 2005). In addition, FAK (Ptk2ab) regulates coronary vessel formation during heart regeneration in adult zebrafish (Missinato et al., 2015). Localized to focal adhesions, FAK interacts with integrin-associated proteins, such as paxillin and talin, and can elicit extracellular signal-regulated kinase (ERK) signaling (Fincham et al., 2000; Hauck et al., 2002; Klemke et al., 1997). Interaction between FAK and the adaptor protein paxillin is crucial for activation of signaling cascades required for cell survival and motility (Turner, 2000). In *Vcl* knockout mice, FAK activity is upregulated (Xu et al., 1998a). In cultured mouse *Vcl* null cells, paxillin and FAK interaction is enhanced and FAK phosphorylation is upregulated (Subauste et al., 2004), suggesting that vinculin regulates cell survival and motility by modulating paxillin-FAK interaction. Nevertheless, cellular functions of vinculin remain to be fully elucidated during heart development.

Here, we report a zebrafish gene-trap mutant *v12*, in which the *vclb* gene is disrupted by a *Tol2* transposon insertion. We found that *vclb* plays crucial roles during coronary vessel development. Vclb is enriched in the epicardium and endocardium and regulates the formation of the coronary vessel network by fine-tuning the phosphorylation of FAK and ERK. Our study in zebrafish uncovered previously unappreciated functions of vinculin in coronary vessel development, and might have implications regarding therapeutic intervention of certain subtypes of coronary heart disease.

RESULTS

The zebrafish V12 gene-trap line displays specific GFP expression in the heart

In a *Tol2* transposon-mediated gene-trap screen in zebrafish, we identified the V12 line, in which the EGFP reporter shows distinct expression patterns in various tissues, including the heart. Specifically, EGFP expression initiates in the somite septum at 24 h post fertilization (hpf). At 35 hpf, EGFP is detected in the heart. From 50 hpf on, EGFP is prominently localized in the ventricle (Fig. 1A-H). Colocalization of EGFP with β-catenin but not with α-actinin (a sarcomere Z-disc marker) suggests that EGFP expression is close to the cell membrane (Fig. 1I-J″). Intercross between heterozygous fish (F1) yielded 908 F2 embryos, which were divided into three groups based on EGFP intensity (no, 23.6%; weak, 52.2%; strong, 24.2%) indicating that alleles of a single locus in the V12 line are segregated at Mendelian ratio. Accordingly, the no, weak and strong EGFP F2 families are likely to represent wild type, heterozygote and homozygote (hereafter referred to as the *v12* mutant), respectively. Strong EGFP expression in hearts suggests involvement of the trapped gene during heart development.

The *vinculin* gene (*vclb*) is disrupted in the V12 line

To identify the trapped gene, we carried out thermal asymmetric interlaced polymerase chain reactions (TAIL-PCR) to amplify the flanking genomic sequences of the *Tol2* insertion site, as previously reported (Liu and Chen, 2007). The flanking sequences were mapped to an unreported sequence in chromosome 12, which encodes a polypeptide with high homology to human VCL protein (Fig. 2A, Fig. S1). There are two *vinculin* genes in the zebrafish genome (Pascoal et al., 2013). *vcla* is located on chromosome 13 and its full-length cDNA has been cloned (Vogel et al., 2009), whereas the sequence of *vclb* is unknown. We cloned the full-length *vclb* cDNA, which encodes a polypeptide of 1065 amino acid residues. The *vclb* RNA expression pattern resembles that of the EGFP reporter in the trap line (Fig. 2B). Unlike *vcla*, *vclb* shows no alternative splicing around the region corresponding to exon 19 in *vcla* (Fig. 2C). The *EGFP-vclb* fusion transcript from the *v12* mutant encodes a chimeric protein with EGFP fused to the N-terminal 261 amino acids of Vclb (NVclb, Fig. 2D). A protein of predicted size (55 kDa) was detected by western blot using a GFP antibody (Fig. 2E). RT-PCR genotyping of embryos of different EGFP intensity confirmed their respective genotypes (Fig. 2F). RT-PCR and qRT-PCR results show that the full-length *vclb* mRNA is almost undetectable, whereas *vcla* is not affected in the homozygous mutant (Fig. 2F,G). Together, these results indicate that *vclb* is disrupted in *v12* mutants.

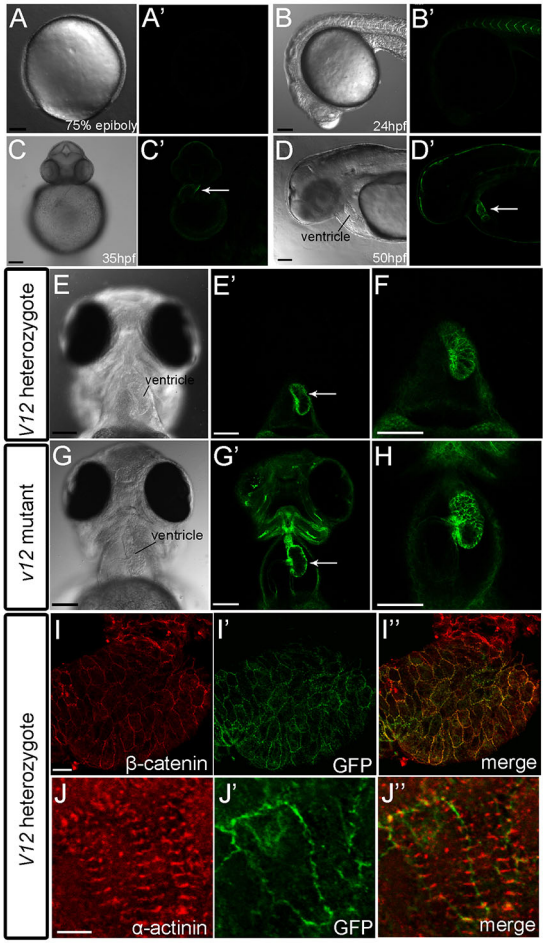

Fig. 1. GFP is highly expressed in the ventricle of *v12* zebrafish embryos. (A-D′) GFP is not detected in 75% epiboly embryos (A,A′), and is initially expressed in the somite boundaries at ~24 hpf (B). Cardiac GFP expression starts at ~35 hpf (C,C′) and GFP is highly expressed in the ventricle at 50 hpf (D,D′). Arrows indicate ventricle. (E-H) Ventricular GFP expression in *v12* heterozygotes (E-F) and *v12* homozygotes (G-H) at 84 hpf shown at high magnification. Arrows indicate ventricle. (I-I″) Immunostaining shows that β-catenin and GFP colocalize close to the cell membrane in *v12* heterozygous hearts at 78 hpf. (J-J″) Immunostaining shows that GFP is absent from Z-disc (α-actinin) in *v12* heterozygous hearts at 78 hpf. Scale bars: 100 µm in A-D,E-H; 20 µm in I; 5 µm in J.

vclb deletion causes lethality at juvenile stages

The viability of *v12* mutants is comparable to that of wild-type and heterozygous embryos for the first 21 days of development. After 21 days post fertilization (dpf), the mutants die off and few survive

Development (2016) 143, 3522-3531 doi:10.1242/dev.132936

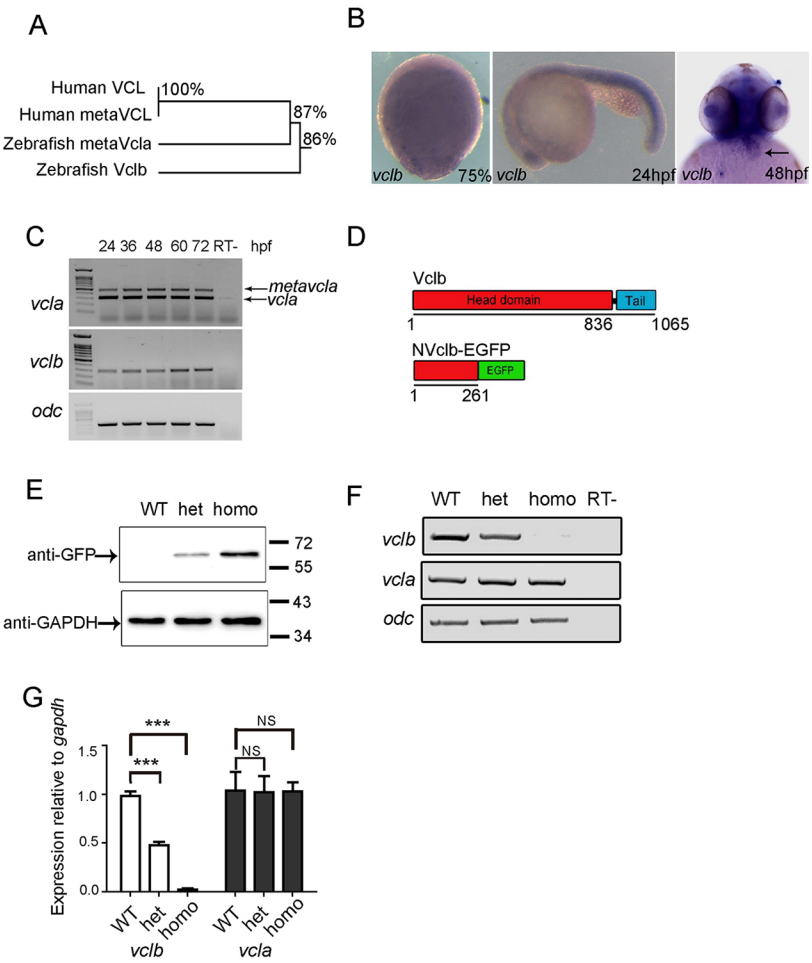

Fig. 2. The *vclb* gene is disrupted in the *v12* mutant. (A) The zebrafish *vclb* gene is a homolog of human vinculin (*VCL*). (B) *vclb* mRNA expression as revealed by *in situ* hybridization is similar to EGFP expression patterns in the somites at 24 hpf and the heart at 48 hpf. Arrow points to the heart. (C) *vclb* is an alternative transcript corresponding to the *vcla* transcript variant without exon 19. No other alternative splicing transcripts are detected. *odc* (*ornithine decarboxylase 1*) is a loading control. RT–, without reverse transcriptase. (D) Diagram indicating that the transposon insertion in the *v12* mutant causes fusion of EGFP with the N-terminal 261 amino acids of Vclb (NVclb). (E) NVclb-EGFP fusion protein expression detected with a GFP antibody in heterozygous and homozygous *v12* mutant heart at 30 dpf. Size markers (kDa) are shown to the right. Gapdh provides a loading control. (F,G) Intact *vclb*, but not *vcla*, mRNA expression is blocked in the *v12* mutant at 36 hpf as assayed by RT-PCR (F) and qRT-PCR (G). The expression level of *vcla* is the same among wild type, heterozygotes and *v12* mutant. The qRT-PCR data are presented as mean±s.e.m. Two-tailed unpaired *t*-test; NS, not significant; ***P<0.001.

beyond 2 months (Fig. S2A). The overall morphology of the mutants is indistinguishable from that of the wild-type or heterozygous siblings until 3.5 dpf, when pericardiac edema is obvious in the mutant (Fig. S2B,C). At 30 dpf, *v12* mutants exhibit a smaller body size (about two-thirds the size of control siblings, Table S1) with craniofacial malformations and pleural effusion (Fig. S2D,E). Adult *vclb* heterozygotes are viable, fertile and indistinguishable from wild type, suggesting that the NVclb-EGFP fusion does not affect the wild-type allele through a dominant-negative effect.

To confirm that *vclb* deficiency causes the observed defects, we used CRISPR-Cas9 technology (Chang et al., 2013; Hwang et al., 2013) and generated a new *vclb* mutant with a 17 bp deletion comprising nucleotides 51 to 67 downstream of the translation initiation site (Fig. S3A). The resulting $vclb^{del17}$ mutants show similar cardiac defects to *v12* mutants (Fig. S3B-O′). Furthermore, the new mutant allele failed to compensate the *vclb* allele in the V12 line. The *v12*/$vclb^{del17}$ double heterozygotes exhibit the same cardiac defects as the individual mutants (data not shown). Together, these results confirm that *vclb* mutation causes the *v12* mutant phenotypes.

vclb regulates epicardial proliferation and differentiation in the ventricles

Pericardiac edema and pleural effusion in the *v12* mutant indicate that cardiac defects occur at juvenile stages. In the *v12* mutant, *vclb* mRNA is greatly reduced in the heart during embryonic stages (Fig. S4A-D). However, the *cmlc2* (*myl7*) and *nkx2.5* genes, which are involved in cardiac progenitor specification, have comparable expression levels in control siblings and *v12* mutant embryos (Fig. S4E-H). During ventricle morphogenesis, the expression levels of *vmhc* and *nppa* in *v12* mutants are also comparable to those in control siblings (Fig. S4I-P). Early development of endocardial and epicardial cells appears normal in the *v12* mutant, as indicated by a *Tg*(*flk1:mcherry*) (*flk1* is also known as *kdrl*) transgenic reporter (Dong et al., 2012) and *tbx18* RNA *in situ* hybridization (Begemann et al., 2002) (Fig. S5). These results suggest that the early specification of cardiac progenitors and the initial development of cardiac chambers are largely normal and that the lethality is due to subsequent chamber differentiation and maturation defects in *v12* mutants.

Next, we examined hearts from *v12* mutants and control siblings at different larval stages. The mutant ventricles change from pyramid-like, as in control siblings, to spherical, resembling those from human DCM patients (Fig. 3A,B). The mutant hearts retain a relatively normal sarcomere structure, but gaps can be seen between some muscle fibers (Fig. S6A-D). In addition, the density of cardiomyocytes increases in the mutant, as indicated by Mef2 (cardiomyocyte nuclear specific) antibody staining (Fig. S6E,F), indicating cardiomyocyte proliferation. Sub-epicardium hemorrhage occurred in ∼30% of *v12* mutant ventricles (Fig. 3C,D, Fig. S7). Moreover, at 30 dpf, epicardial cells in *v12* mutants exhibit cobblestone-like shapes (Fig. 3F,H) that clearly differ from the squamous epithelium of serrated cell membrane morphology in wild-type siblings (Fig. 3E,G). In wild-type ventricles, only a single layer of epicardial cells expressing Aldh1a2 exists (Fig. 3I). By contrast, in

Development (2016) 143, 3522-3531 doi:10.1242/dev.132936

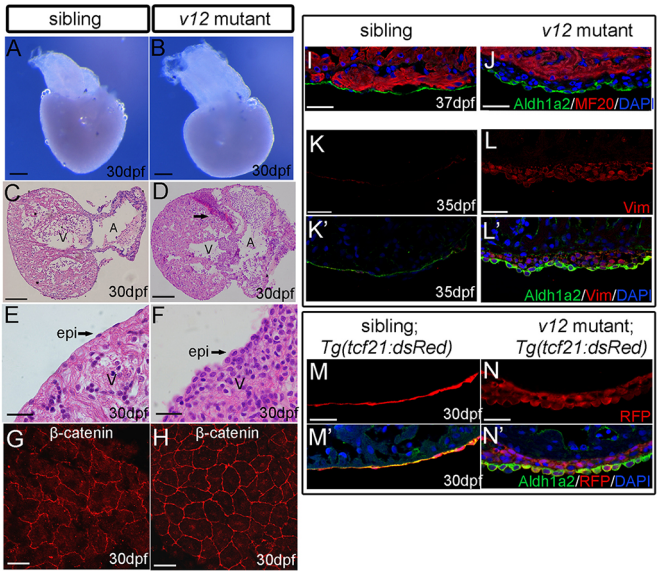

Fig. 3. Overproliferation of Tcf21-positive epicardial-derived cells in *v12* mutants. (A,B) Ventricular morphology (dorsal view) of the *v12* mutant and a wild-type sibling at 30 dpf. Note the spherical ventricles in the *v12* mutant (B) as compared with the pyramid-like heart in wild type (A). (C-F) Histology of the *v12* mutant (D,F) and its wild-type sibling (C,E), showing the malformed heart and sub-epicardial hemorrhage (arrow) in the mutant. Epicardial cells (epi) change from wild-type squamous epithelium (E) to oval-shaped in the *v12* mutant (F). (G,H) β-catenin immunostaining marks the cell membrane of epicardial cells. Cell size is reduced and the cell boundary is smoother in the mutant (H) compared with the wild-type sibling (G). (I,J) MF20 staining shows that the overproliferated cells in the sub-epicardium of the *v12* mutant are negative for muscle-specific myosin heavy chain. (K-L′) The overproliferated cells are positive for vimentin (a marker of mesenchymally derived cells) in the *v12* mutant (L,L′) compared with its control sibling (K,K′). Aldhla2 marks the epicardium. (M-N′) Aldh1a2 colocalizes with *Tg*(*tcf21:dsRed*) transgenic reporter in the epicardial cells of the wild-type sibling at 30 dpf (M,M′). By contrast, both overproliferated cells in the sub-epicardium region and the outermost layer of epicardial cells are positive for DsRed staining. Only the outermost layer of epicardial cells shows strong Aldh1a2 staining in the mutant (N,N′). A, atrium; V, ventricle. Scale bars: 100 µm in A-D; 20 µm in E-N.

the *v12* mutant, in addition to one layer of Aldh1a2-positive epicardial cells, two to three extra layers of vimentin-positive cells fill in the sub-epicardial space (Fig. 3E,F,I-L′). We also used a *Tg*(*tcf21:dsRed*) transgene (Kikuchi et al., 2011) to label the epicardial lineage and found that these extra cells were DsRed-positive but negative for cardiac myosin heavy chain as detected by MF20 antibody staining, suggesting that they were fibroblasts derived from epicardium (Fig. 3I,J,M-N′). An overall increase in Pcna-positive cells is obvious in the *v12* mutant at 15 dpf compared with wild type, but the increase is especially pronounced in the epicardium, confirming the overproliferation observation (Fig. S8). We conclude that Vclb deficiency causes overproliferation and differentiation of epicardial-derived cells.

vclb deficiency causes coronary vessel disorganization

Epicardial cells are involved in coronary vessel development (Dettman et al., 1998; Reese et al., 2002; Vrancken Peeters et al., 1999). Overproliferation of epicardial-derived cells in the *v12* mutant could lead to abnormal coronary vessel development. To better examine possible roles of *vclb* in coronary vessel development, we first investigated its expression pattern in *v12* and sibling hearts using the NVclb-EGFP fusion reporter. NVclb-EGFP is ubiquitously distributed on the ventricle surface (epicardium) and EGFP-positive cells are most abundant in plexus-like structures and in the sub-epicardial region. The EGFP signal is particularly elevated in the mutant (0-9.2 µm from the surface) compared with heterozygotes (0-4.6 µm from the surface) (Fig. 4A-D). In the inner myocardium, EGFP expression is located at the boundary between endocardial cells and muscle cells in both mutants (13.8 µm from the surface) and heterozygotes (9.8 µm from the surface) (Fig. 4E,F). Expression of NVclb-EGFP in epicardial cells was also confirmed by co-immunostaining of myosin heavy chain (MF20) and EGFP in cryosections of ventricles from heterozygotes and *v12* mutants (Fig. 4G-H‴). Expression of NVclb-EGFP at the muscle-endocardium boundary was also shown by co-immunostaining of mCherry and EGFP in cryosections of ventricles from heterozygotes and *v12* mutants in the *Tg*(*flk1:mcherry*) background (Fig. 4I-J′).

We then examined whether *vclb* plays a role in coronary vessel development using the *Tg*(*fli1a:EGFP*) transgenic reporter to label coronary endothelial cells (Roman et al., 2002). Owing to much stronger signals of *Tg*(*fli1a:EGFP*) than of NVclb-EGFP (Fig. S9), we were able to follow coronary vessels by *Tg*(*fli1a:EGFP*) in the compound *Tg*(*fli1a:EGFP*); *v12*(*NVclb-EGFP*) zebrafish.

Similar to the previous mouse study (Red-Horse et al., 2010), in zebrafish the coronary vessels first appear on the dorsal surface of the ventricles near the atrium-ventricle connection at ∼28 dpf (Fig. 5A,E). The coronary vessels then spread over the entire dorsal surface and extend gradually to cover the ventral surface from 35 to 55 dpf (Fig. 5B-D,F-H). New vessels initially appear as isolated blood plexuses that subsequently connect to each other to form a network. This is similar to zebrafish coronary vessel development as described by Harrison et al. (2015). Compared with wild-type siblings, the *v12* mutant has more blood plexuses and vessels at initiation stages (Fig. 5I,M). The blood vessel density in *v12* mutants is higher than that in the control siblings (Fig. S10E). However, *v12* mutants show abundant but disorganized vessels in the ventricle when the wild-type siblings have already formed well-connected coronary vasculatures (Fig. 5J-L,N-P). Blood cells can be seen in some of the coronary vessels of the *v12* mutant (Fig. S11). At 55 dpf, co-immunostaining with EGFP and MF20 antibodies showed that Fli1a-EGFP-positive coronary vessels are in contact with the myocardium in the wild-type ventricle, evidently in the compact myocardium (Fig. 5Q,Q′, arrows). By contrast, coronary vessels in the mutants are surrounded by extra epicardial-derived cells in the sub-epicardial space and most of the vessels are not in contact with cardiac muscle (Fig. 5R,R′, arrows). Together, these results strongly suggest that *vclb* deficiency causes disorganization of the coronary vessels and that abnormal epicardial cell proliferation/differentiation contributes to the coronary vessel defects in *v12* mutants.

In zebrafish, coronary endothelial cells are covered by pericyte-like mural cells and myosin light chain kinase-positive smooth muscle cells (González-Rosa et al., 2011; Hu et al., 2001; Kim et al., 2010). Previous studies showed that Tcf21-positive epicardial cells contribute to progenitors of coronary vessel perivascular cells in zebrafish (Kikuchi et al., 2011). To test whether the overproliferation of epicardial cells affects interactions between coronary endothelial cells and perivascular cells, we used *Tg*(*fli1a:EGFP*) and *Tg*(*tcf21:DsRed*) transgenes to label endothelial (EGFP) and epicardial (dsRed) cells (Kikuchi et al., 2011), respectively. Unlike wild-type embryos, in which endothelial cells are well aligned with dsRed-positive cells, most *v12* mutants show disorganization of increased numbers of perivascular cells, probably owing to mispatterned coronary vessels (Fig. 5S-V″).

Development (2016) 143, 3522-3531 doi:10.1242/dev.132936

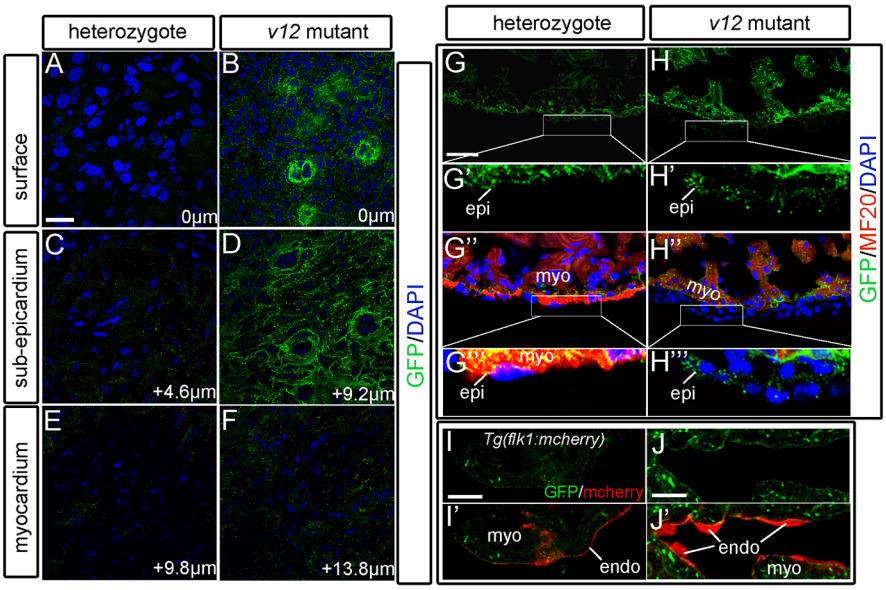

Fig. 4. Ventricular expression patterns of the NVclb-EGFP fusion protein. (A,B) GFP expression in the ventricle surface (0 μm) at 52 dpf, showing the formation of plexus-like structures in the *v12* mutant (B) compared with heterozygotes (A). (C,D) GFP expression patterns in the sub-epicardium of ventricles at 4.6 μm (C) and 9.2 μm (D) from the surface. Strong expression of GFP fusion protein is shown in the mutant (D) compared with heterozygotes (C). (E,F) GFP is detected at the boundary between endothelial cells and muscles of ventricles at 9.8 μm (E) and 13.8 μm (F) from the surface. (G-H‴) GFP is ubiquitously expressed in the ventricle. GFP expression is detected in several layers of GFP^{+}/MF20^{-} epicardium-derived cells in the mutant (H″,H‴) compared with a single layer of epicardial cells in heterozygotes (G″,G‴). (I-J′) *Tg(flk1:mcherry)* transgenic reporter is used to label endothelial cells. GFP is detected at the boundary between endothelial cells (red) and myocardium. endo, endocardium; epi, epicardium; myo, myocardium. Scale bars: 10 μm in A-F,I-J′; 20 μm in G,G″,H,H″.

From these results, we conclude that *vclb* deficiency causes disorganization of the coronary vasculature. Moreover, *vclb* deficiency causes overproliferation of epicardial-derived cells and the disorganization of endothelial cells and perivascular cells.

Vclb deficiency activates ERK and FAK in epicardium and endocardium

The overproliferation of epicardial cells and endothelial cells in *v12* mutant hearts indicates that they are mitotically active. There are a number of mechanisms underlying cell proliferation. For example, growth factor-activated cell proliferation can be mediated by ERK (mitogen-activated protein kinase, MAPK) activity (Seger and Krebs, 1995). We examined ERK activation in zebrafish heart using a phosphorylation-specific ERK antibody. We found a stronger phosphorylated (p) Erk1/2 (Mapk3/1) signal in coronary endothelial cells than in the endocardium of wild type at 55 dpf (Fig. 6A,A′), suggesting that relatively high ERK activity in coronary endothelial cells might be required for coronary vessel development. When treated with 10 μM MEK1 inhibitor U0126 from 28 dpf, coronary vessel development was significantly impaired in the wild-type siblings at 40 dpf (Fig. S10E). pErk1/2 levels were markedly increased in the epicardium and endocardium in *v12* mutants compared with control siblings at 15 and 55 dpf (Fig. 6A-F′). It should be noted that ERK activation occurs at 15 dpf, long before the formation of coronary vessels, indicating that the activation is not a result of myocardial hypoxia. This was confirmed by examining RNA expression of hypoxia markers *hypoxia-inducible factor 1a* (*hif1a*) and *egl-9 family hypoxia-inducible factor 3* (*egln3*, the zebrafish homolog of *prolyl hydroxylase 3*) (Kaelin and Ratcliffe, 2008; Manchenkov et al., 2015) in *v12* and control sibling hearts (Fig. S12).

Previous studies indicated that loss of vinculin enhances the interaction between paxillin and FAK, which results in upregulation of FAK phosphorylation and in turn activates ERK in mouse F9 embryonic carcinoma cells (Subauste et al., 2004; Xu et al., 1998a). We investigated whether similar events occur in *v12* mutant zebrafish hearts, especially in coronary and endocardial endothelial cells. The major paxillin-binding motif of vinculin is known to be located in its C-terminal region (Wood et al., 1994). Indeed, when expressed in HEK293 cells, the remaining NVclb-EGFP fusion protein is not associated with zebrafish paxillin (Fig. 6G), suggesting that paxillin is released from the Vclb protein complex *in vivo*. Immunostaining results also show that the majority of paxillin is no longer localized at the boundary between epicardium and myocardium (Fig. 6H-I′). Release of paxillin may enhance its interaction with FAK to increase FAK phosphorylation. As expected, FAK phosphorylation at Y576/577 is increased in epicardial cells, coronary and endocardial endothelial cells in *v12* mutants compared with wild-type siblings, whereas total FAK is comparable between them (Fig. 6J-M). It should be noted that FAK is not activated in the myocardium, even though Vclb is ubiquitously expressed in the ventricle (Fig. 4).

We identified a monoclonal antibody against human VCL that recognizes endogenous Vcla proteins but not NVclb-EGFP proteins (Fig. 7A). We noted that Vcla expression levels are similar between control siblings and *v12* mutants (Fig. S13). Whereas NVclb-EGFP is expressed in both myocardium and epicardium (Fig. 7B-B‴), Vcla is mainly expressed in the myocardium (Fig. 7C-C‴). The sequences of Vcla and Vclb are highly conserved and the proteins are likely to be functionally redundant. The lack of FAK activation in the myocardium of *v12* mutants might therefore be due to Vcla expression there (Fig. 7C-C‴).Thus, complete lack of vinculin activity in the epicardium causes the elevation of pFAK and pERK.

DISCUSSION

Previously, vinculin was shown to be crucial for myocardium morphogenesis. In *Vcl* knockout mice, the myocardial structure is severely reduced (Xu et al., 1998a). Furthermore, *VCL* mutations have been identified in a subset of human DCM patients. Mechanistically, disruption of intercalated disc structure and an abnormal distribution of cell-junction proteins in cardiac muscle were found in one of these DCM patients and in cardiomyocyte-specific *Vcl* knockout mice (Olson et al., 2002; Zemljic-Harpf et al., 2007). In addition to cardiac muscle, VCL and metaVCL are also expressed in non-muscle cells (Belkin et al., 1988; Koteliansky et al., 1992). Vinculin functions in other tissues remain largely unknown. We show here that two *vclb* mutants have identical multiple cardiac defects, especially in epicardial differentiation and subsequent coronary vessel development. Vclb deficiency increases the phosphorylation of Erk1/2 and FAK in endothelial cells and epicardial cells, resulting in the overproliferation of epicardial-derived cells and abnormal coronary vessel development. Our

Development (2016) 143, 3522-3531 doi:10.1242/dev.132936

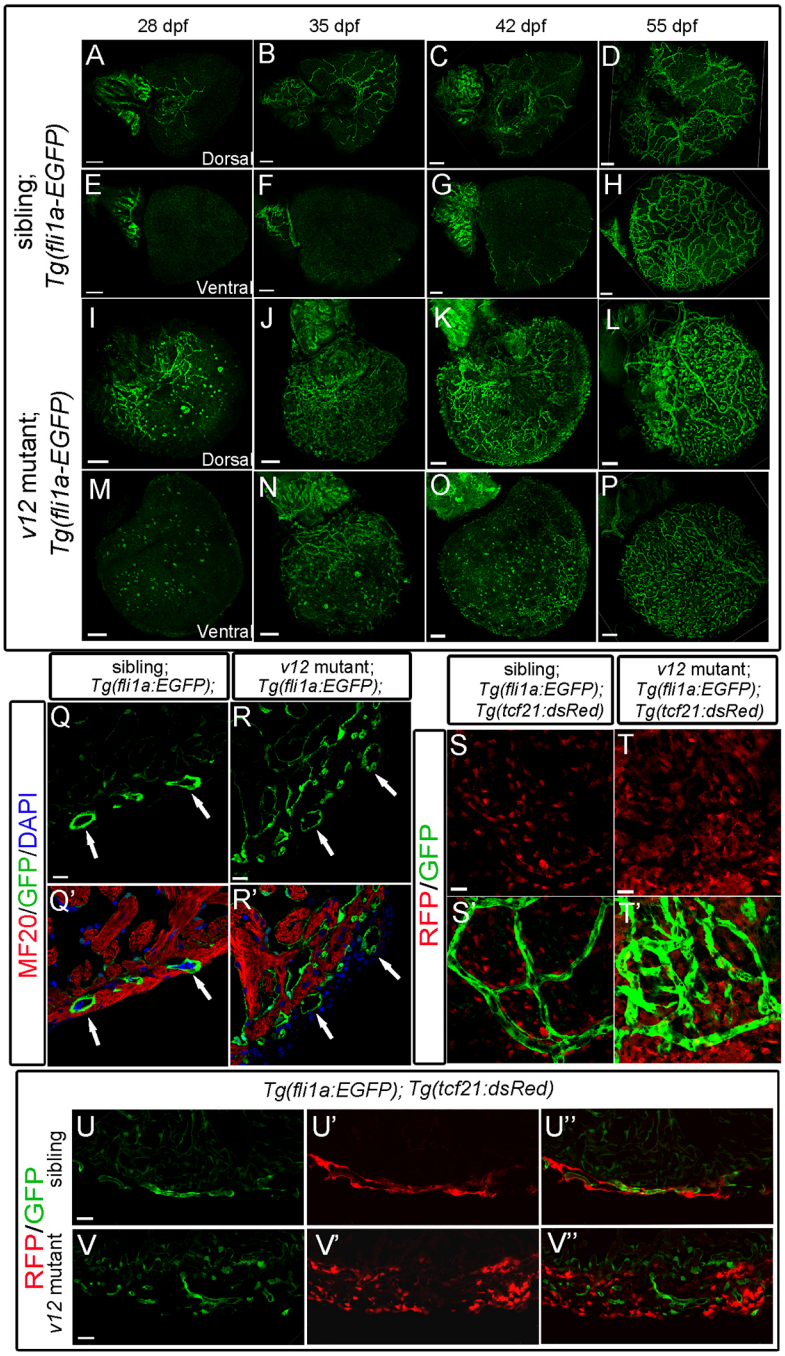

Fig. 5. *vclb* deficiency causes disorganization of coronary vessels. The *Tg*(*fli1a:EGFP*) transgenic line (endothelial cells labeled by EGFP) is used to trace coronary vessel development. The *Tg*(*tcf21:dsRed*) transgenic line is used to label epicardial cells. (A-H) In wild-type hearts, coronary vessels first appear on the dorsal surface of the ventricle and are close to the atrium-ventricle connection at ∼28 dpf. Coronary vessels then spread, extend, and wrap the entire ventricle wall from 35 to 55 dpf. Dorsal views (A-D) and ventral views (E-H) are shown. (I-P) In the *v12* mutant, coronary vessels appear at the same place as in wild-type siblings, but more vessels are detected at the initial stages. Wild-type coronary vessels are well connected to each other, but the overproliferated mutant vessels remain isolated and disorganized. Dorsal views (I-L) and ventral views (M-P) are shown. (Q-R′) In the *v12* mutant, coronary vessels are surrounded by epicardial-derived cells (R,R′) rather than by cardiac muscles as in the wild-type sibling (Q,Q′) at 55 dpf. MF20 stains cardiac muscles. Arrows indicate vessels that are (Q,Q′) or are not (R,R′) in contact with cardiac muscle. (S-V″) At 40 dpf, *Tg*(*fli1:EGFP*)-labeled endothelial tubes in wild-type ventricles are well aligned with *Tg*(*tcf21:dsRed*)-labeled epicardial-derived perivascular cells (S,S′,U-U″). By contrast, most of the endothelial tubes in *v12* mutants are not well aligned with perivascular cells (T,T′,V-V″). Note the overproliferated endothelial and perivascular cells in the mutant. Results are shown in whole-mount view (S-T′) and cryosection (U-V″). Scale bars: 100 µm in A-P; 10 µm in Q-R′; 20 µm in S-V″.

results exemplify crucial functions of the cytoskeletal protein vinculin in heart development.

The human *VCL* gene is located on chromosome10. Alternative splicing of exon 19 generates the two isoforms VCL and metaVCL. Human DCM-related mutations all map to exon 19 of *VCL* (Olson et al., 2002). It should be noted that human DCM patients are heterozygous for the *VCL* mutations, suggesting that homozygous mutants are lethal. metaVCL, which contains additional amino acids from exon 19, is specifically expressed in cardiac muscle and so its major function is likely to be cardiac muscle specific. In *Vcl* knockout mice both vinculin isoforms are disrupted, making it difficult to distinguish any different roles of the two isoforms (Xu et al., 1998a). By contrast, *vcla* and *vclb* are two separate genes in zebrafish. While *vcla* has two splicing isoforms similar to its human homolog, the zebrafish *vclb* transcript resembles the human short isoform. In *v12* mutants, *vcla* expression remains high in the myocardium (Fig. 7), which masks the loss of Vclb due to their functional redundancy. The different genomic organizations of the vinculin genes in human and zebrafish explain why we were able to uncover Vclb-specific functions in zebrafish endocardial/endothelial and epicardial cells. We speculate that the phenotypic difference between complete knockout (embryonic lethal) and cardiomyocyte-specific deletion (survival to adulthood) of the *Vcl* gene in mouse might be due to its expression and essential functions in endocardial/endothelial and epicardial cells. Specific deletion of the mouse *Vcl* gene in these cells can be used to test this hypothesis.

FAK promotes angiogenesis in tumor formation (Zhao and Guan, 2011). FAK kinase activity and Grb2/ERK signaling are required

Development (2016) 143, 3522-3531 doi:10.1242/dev.132936

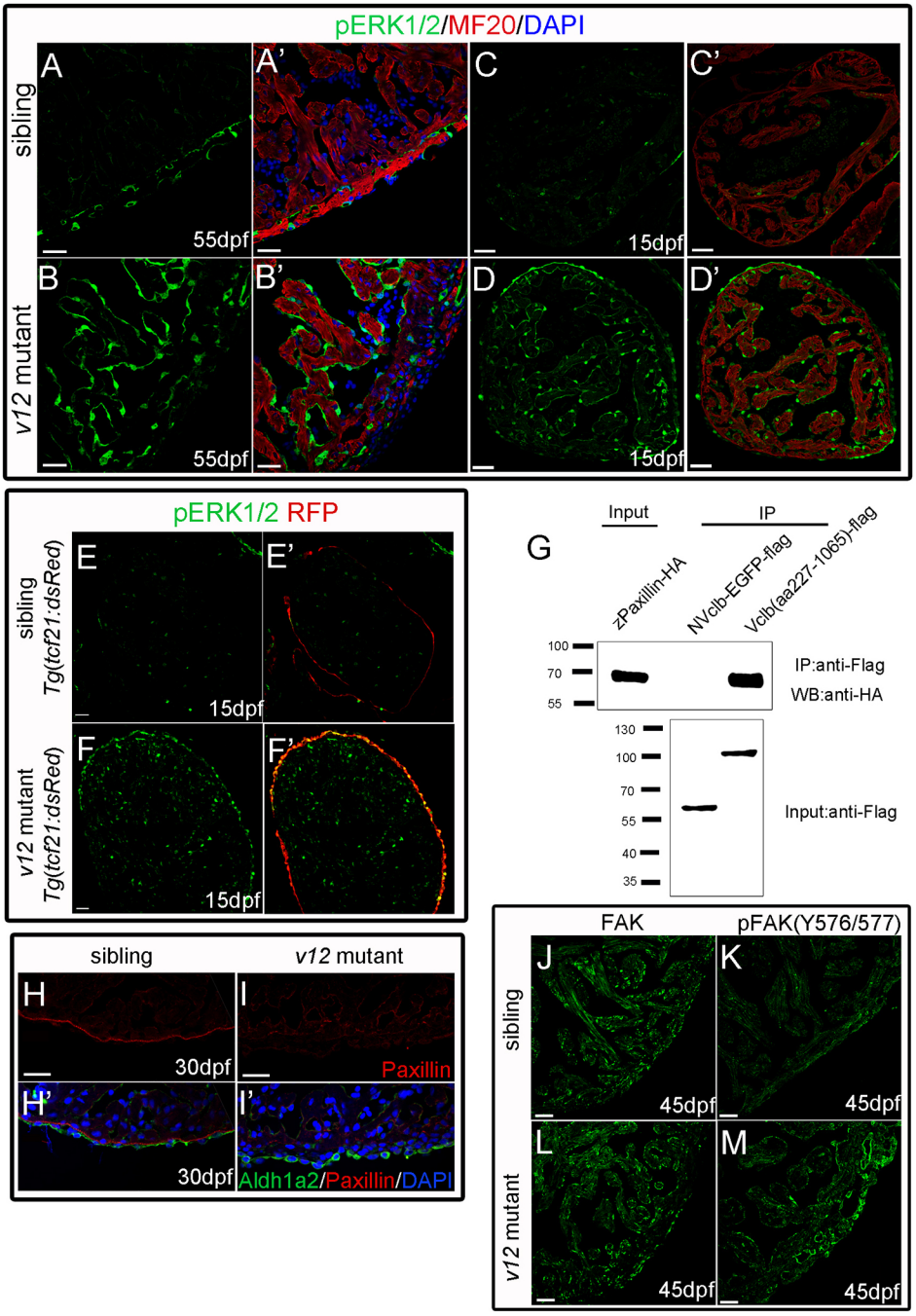

Fig. 6. pERK and pFAK are upregulated in the epicardium and endocardium of *v12* mutant ventricles. (A-B′) pErk1/2 expression (green) is increased in the endocardium of *v12* mutants at 55 dpf compared with wild-type sibling. (C-D′) pErk1/2 expression is increased in the epicardium and endocardium of *v12* mutant at 15 dpf. MF20 staining (red) indicates cardiac muscles. (E-F′) *Tg*(*tcf21:dsRed*) transgenic reporter indicates epicardium. Upregulated pErk1/2 colocalizes with RFP signal. (G) Co-immunoprecipitation shows that NVclb-EGFP is not associated with paxillin, which normally interacts with wild-type Vclb, when ectopically expressed in HEK293 cells. IP, immunoprecipitation; WB, western blot. Size markers (kDa) are shown to the left. (H-I′) The localization of paxillin at the boundary between epicardium and myocardium is partially lost in the *v12* mutant (L,L′) compared with wild-type siblings (H,H′). (J-M) pFAK(Y576/577) expression is upregulated whereas total FAK expression remains unchanged in the epicardium and endocardium of the *v12* mutant at 45 dpf (L,M) compared with wild-type sibling (J,K). Scale bars: 20 µm.

for VEGF secretion acting downstream of activated Src kinase in breast carcinoma cells (Mitra et al., 2006). The blood vessel hyperplasia in the *v12* mutant suggests that ERK/FAK activation might play a role in the process. Indeed, during coronary vessel formation, levels of Erk1/2 phosphorylation were upregulated in coronary endothelial cells compared with the endocardium (Fig. 6A). This suggests that activation of ERK is required for epicardial- and endocardial-derived cells to form coronary vasculature, which is consistent with the role of ERK activation in cell proliferation and migration (Cho and Klemke, 2000). When treated with 10 µM MEK1 inhibitor U0126 from 28 dpf, coronary vessel development was significantly impaired in wild-type siblings at 40 dpf, but U0126 at this concentration could not alleviate the coronary vessel hyperplasia in *v12* mutants (Fig. S10E). Concentrations above 10 µM cause lethality within 24 h, which might be caused by other organ failures owing to their higher sensitivity to the MEK1 inhibitor. Coronary vessel development includes both vasculogenesis and angiogenesis. Vclb deficiency does not appear to affect initial vasculogenesis, but impacts blood vessel connection such that they fail to form a well-organized network of coronary vasculatures. It is likely that coronary progenitor cells and ECM adhere to form cell-cell adhesions and focal adhesions at the end of cell migration. During this process, vinculin not only functions in the assembly of focal adhesion structures, but also helps to downregulate ERK phosphorylation to maintain a balanced level of coronary angiogenesis, possibly through modulating paxillin-FAK interaction. In *v12* mutants, this balance is disrupted and hyperactivated ERK causes overproliferation of endocardial- and epicardial-derived cells, including pericytes, leading to abnormal

Development (2016) 143, 3522-3531 doi:10.1242/dev.132936

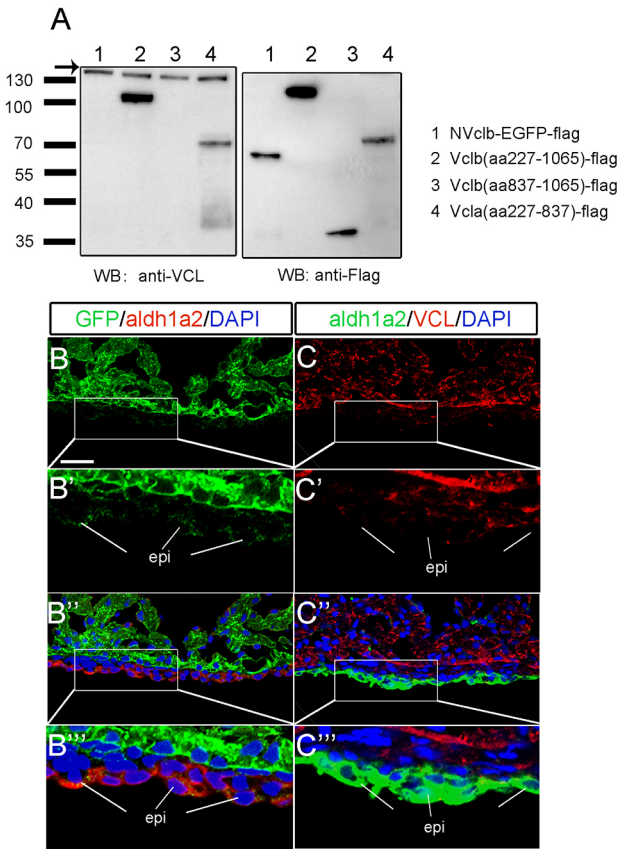

Fig. 7. Vcla expression may alleviate defects in myocardium in the *v12* mutant. (A) The monoclonal anti-VCL antibody fails to recognize the NVclb-EGFP fusion protein and C-terminal Vclb but recognizes Vclb (aa227-1065) (left panel). All three Vclb variants can be detected by anti-FLAG antibody (right panel). The anti-VCL antibody recognizes the middle region of Vclb, which is absent from NVclb-EGFP, and recognizes Vcla protein (aa227-837), indicating that the VCL antibody only recognizes Vcla protein in *v12* mutants. Arrow points to the endogenous VCL protein of HEK293 cells. (B-B‴) Immunostaining reveals that NVclb-EGFP colocalizes with Aldh1a2 in epicardial cells in *v12* mutant ventricles at 50 dpf. (C-C‴) Immunostaining shows that Vcla is mainly expressed in the myocardium but not in epicardial cells in *v12* mutant ventricles at 50 dpf.

alignment and interaction of endothelial cells and pericytes in the vessel wall, as well as improper interaction of vessels with the myocardium.

Previous results indicated that overexpression of the 258 amino acid N-terminal fragment of Vcl protein in vinculin null cells causes more stable focal adhesions than full-length Vcl (Carisey et al., 2013; Humphries et al., 2007; Xu et al., 1998b). We note that *v12* mutants retain the N-terminal 261 amino acids, but the *vclb* heterozygotes show no obvious developmental defects. To exclude possible roles of the N-terminal fragment in *v12* mutants, we also generated a *vclb* null mutant, *vclb*^{del17}, using CRISPR-Cas9 technology. *vclb*^{del17} mutants exhibit similar cardiac phenotypes to *v12* mutants, including pleural effusion and epicardial overproliferation (Fig. S3). Thus, the phenotypes of the *v12* mutant are caused by loss of function rather than by other mechanisms such as dominant-negative interference.

Epicardial cell activation also plays a key role in heart regeneration. Adult zebrafish hearts can regenerate after damage, making it an excellent model for the study of heart regeneration (Major and Poss, 2007; Poss et al., 2002). During zebrafish heart regeneration, reactivated epicardial cells migrate into wound sites and differentiate into fibroblasts and pericyte-like cells (González-Rosa et al., 2012; Kikuchi et al., 2011; Lepilina et al., 2006). FGF and H_2O_2 signaling are crucial to fine-tune the phosphorylation of ERK and to control both myocardial and coronary vessel regeneration (Han et al., 2014; Lepilina et al., 2006). The role of vinculin-pFAK-pERK in regulating epicardial and coronary vessel development, as reported here, will enhance our understanding of the molecular basis of heart regeneration.

MATERIALS AND METHODS

Zebrafish strains and gene trapping

The zebrafish AB line was used in this study. Zebrafish husbandry and embryo manipulations were performed as described (Westerfield, 2000). The experimental procedures in this study have been approved by the Animal Ethical Committee of the Institute of Genetics and Developmental Biology, Chinese Academy of Sciences. The gene-trap vector and procedure were described previously (Liu et al., 2012). Over 300 injected embryos were raised and outcrossed with wild-type fish. EGFP expression was examined under a fluorescence microscope at different developmental stages until 96 hpf. Sixteen gene-trap lines with obvious EGFP expression were identified. The V12 line, which is one of the trapped lines, was maintained by crossing the heterozygotes with wild-type fish to avoid inbreeding depression for all experiments described here.

Tg(*flk1:mcherry*) (Dong et al., 2012) and *Tg*(*fli1a:EGFP*) (Roman et al., 2002) were obtained from Dr Feng Liu (Chinese Academy of Sciences, Beijing). *Tg*(*tcf21:dsRed*) (Kikuchi et al., 2011) was obtained from Dr Geoffrey Burns (Massachusetts General Hospital, Boston). *vclb*^{del17}, which carries a 17 bp deletion near the ATG of the *vclb* gene, was created using CRISPR-Cas9 technology as previously reported (Chang et al., 2013; Hwang et al., 2013).

TAIL-PCR, RT-PCR and RT-qPCR

To identify the entrapped gene in the *v12* mutant, we used TAIL-PCR to clone the genomic sequences upstream and downstream of the transposon insertion site as reported (Liu and Chen, 2007). These genomic sequences were used to design genotyping primers. The primers used in TAIL-PCR and genotyping are shown in Table S2. For RT-PCR, total RNA was isolated from ten embryos each of wild type, heterozygote and *v12* mutant at the indicated stages using TRIzol reagent (Life Technologies). The first-strand cDNA was synthesized with M-MLV reverse transcriptase (Life Technologies). RT-qPCR was performed in the Bio-Rad CFX96 system. The full-length *vclb* mRNA sequence was cloned (GenBank KT862534) and used to design the primers shown in Table S3. The primer sequences of *egln3* were described previously (Manchenkov et al., 2015).

Quantitative analysis of cardiomyocyte and coronary vessel density

All quantifications were performed using high-resolution confocal images and ImageJ software. Calculations employed GraphPad Prism software. Statistical analysis was performed by unpaired, two-tailed Student's *t*-test. For all bar graphs, data are represented as mean±s.e.m. $P<0.05$ was considered significant.

For measurement of cardiomyocyte density, two randomly chosen fields were used to quantify the number of Mef2-positive nuclei and MF20-positive areas in immunostained ventricle sections of 35 dpf samples. We calculated the ratio of Mef2-positive nuclei to the MF20-positive area of the field (175 µm×175 µm), and calculated the density as the number of Mef2-positive nuclei (cardiomyocytes) per 1 mm^2. Each group contained five hearts. Measurement of coronary vessel density was performed as described previously (Wilhelm et al., 2016). Randomly chosen fields were used to quantify vascularization at the ventricle surface (40 dpf). Endothelial coverage was determined by calculating the ratio of the GFP-positive area to the total area of the field (200 µm×200 µm), and was expressed as a percentage of the area covered by GFP-positive endothelial cells. Each group contains five hearts with four fields (two on the dorsal and two on the ventral side) from each heart.

Development (2016) 143, 3522-3531 doi:10.1242/dev.132936

RNA *in situ* hybridization

Digoxigenin-labeled or fluorescein-labeled probes were synthesized using an *in vitro* transcription system (Roche). Whole-mount *in situ* hybridization was performed as described (Thisse and Thisse, 2008). BM Purple (Roche) was used to visualize RNA signal at room temperature. Cryosection *in situ* hybridization was performed as described previously (Simmons et al., 2007).

Western blotting and immunofluorescence

To detect the NVclb-EGFP protein and Vcl protein expression, primary antibodies used in western blotting were rabbit polyclonal anti-GFP (1:2000; Abcam, ab290) and mouse monoclonal anti-VCL (1:5000; Sigma, V9131). For immunoprecipitation experiments, the primary antibodies used in western blot were rabbit polyclonal anti-HA (1:2000; EasyBio, BE 2008), mouse monoclonal anti-FLAG (1:2000; Sigma, F3165) and anti-FLAG M2 affinity gel (1:100; Sigma, A2220). Whole-mount immunofluorescence assay of dissected heart was performed as described (Yang and Xu, 2012). Embryos were photographed with an Olympus FV1000 confocal microscope.

For immunofluorescence staining, samples were fixed with 4% paraformaldehyde overnight at 4°C, washed with PBST (PBS with 0.1% Tween 20), and embedded in paraffin. Sections (5 µm) were then rehydrated and incubated overnight at 4°C with primary antibody in blocking solution followed by an Alexa Fluor 594 goat anti-mouse or Alexa Fluor 488 goat anti-rabbit secondary antibody (1:1000; Life Technologies). DAPI was used to stain nuclei. Primary antibodies were rabbit monoclonal anti-pFAK (pY576/577) (1:100; Invitrogen, 44-652G), rabbit polyclonal anti-β-catenin (1:200; Abcam, ab6302), rabbit monoclonal anti-pErk1/2 (1:400; Cell Signaling Technology, 4370), rabbit polyclonal anti-Aldh1a2 (1:200; GeneTex, GTX124302), rabbit polyclonal anti-Mef2 (1:50; Santa Cruz, sc-313), mouse monoclonal anti-α-actinin (sarcomeric) (1:200; Sigma, A7811), anti-myosin heavy chain monoclonal MF20 (1:200; Developmental Studies Hybridoma Bank, Iowa), mouse monoclonal anti-VCL (1:200; Sigma, V9131), mouse monoclonal anti-Pcna (1:100; Sigma, clone PC10), rabbit polyclonal anti-Pcna (1:100; Santa Cruz, sc-7907), mouse monoclonal anti-mCherry (1:100; EasyBio, BE2026), mouse monoclonal anti-GFP (1:100; EasyBio, BE2001) and rabbit monoclonal anti-GFP (1:100; Cell Signaling Technology, 2956). Sections were photographed with the Olympus FV1000 confocal microscope.

Acknowledgements

We thank members of J.Z. and J.X. laboratories for help and discussions; Dr Koichi Kawakami for the original *Tol2* system; Dr Chao Liu for the modified *Tol2* system; and Dr Feng Liu for providing *Tg*(*fli1a:EGFP*) and *Tg*(*flk1:mcherry*) transgenic lines.

Competing interests

The authors declare no competing or financial interests.

Author contributions

F.C., L.M., Q.W., X.G. performed experiments; F.C. , J.X. and J.Z. analyzed data; F.C. prepared figures; F.C., J.X. and J.Z. designed experiments and wrote the paper.

Funding

This work was financially supported through grants from the National Natural Science Foundation of China [31471359, 31590830]; the Ministry of Science and Technology of the People's Republic of China [2013CB945000]; and the Chinese Academy of Sciences [XDA01010108].

Data availability

The complete cDNA sequence of *Danio rerio vinculin b* is available at GenBank under accession number KT862534.

Supplementary information

Supplementary information available online at
http://dev.biologists.org/lookup/doi/10.1242/dev.132936.supplemental

References

Begemann, G., Gibert, Y., Meyer, A. and Ingham, P. W. (2002). Cloning of zebrafish T-box genes tbx15 and tbx18 and their expression during embryonic development. *Mech. Dev.* **114**, 137-141.

Belkin, A. M., Ornatsky, O. I., Glukhova, M. A. and Koteliansky, V. E. (1988). Immunolocalization of meta-vinculin in human smooth and cardiac muscles. *J. Cell Biol.* **107**, 545-553.

Braren, R., Hu, H., Kim, Y. H., Beggs, H. E., Reichardt, L. F. and Wang, R. (2006). Endothelial FAK is essential for vascular network stability, cell survival, and lamellipodial formation. *J. Cell Biol.* **172**, 151-162.

Carisey, A. and Ballestrem, C. (2011). Vinculin, an adapter protein in control of cell adhesion signalling. *Eur. J. Cell Biol.* **90**, 157-163.

Carisey, A., Tsang, R., Greiner, A. M., Nijenhuis, N., Heath, N., Nazgiewicz, A., Kemkemer, R., Derby, B., Spatz, J. and Ballestrem, C. (2013). Vinculin regulates the recruitment and release of core focal adhesion proteins in a force-dependent manner. *Curr. Biol.* **23**, 271-281.

Chang, N., Sun, C., Gao, L., Zhu, D., Xu, X., Zhu, X., Xiong, J.-W. and Xi, J. J. (2013). Genome editing with RNA-guided Cas9 nuclease in zebrafish embryos. *Cell Res.* **23**, 465-472.

Cho, S. Y. and Klemke, R. L. (2000). Extracellular-regulated kinase activation and CAS/Crk coupling regulate cell migration and suppress apoptosis during invasion of the extracellular matrix. *J. Cell Biol.* **149**, 223-236.

Dettman, R. W., Denetclaw, W., Jr., Ordahl, C. P. and Bristow, J. (1998). Common epicardial origin of coronary vascular smooth muscle, perivascular fibroblasts, and intermyocardial fibroblasts in the avian heart. *Dev. Biol.* **193**, 169-181.

Dong, W., Yang, Z., Yang, F., Wang, J., Zhuang, Y., Xu, C., Zhang, B., Tian, X.-L. and Liu, D. (2012). Suppression of Rap1 impairs cardiac myofibrils and conduction system in zebrafish. *PLoS ONE* **7**, e50960.

Fincham, V. J., James, M., Frame, M. C. and Winder, S. J. (2000). Active ERK/MAP kinase is targeted to newly forming cell-matrix adhesions by integrin engagement and v-Src. *EMBO J.* **19**, 2911-2923.

Geiger, B. (1979). A 130K protein from chicken gizzard: its localization at the termini of microfilament bundles in cultured chicken cells. *Cell* **18**, 193-205.

González-Rosa, J. M., Martin, V., Peralta, M., Torres, M. and Mercader, N. (2011). Extensive scar formation and regression during heart regeneration after cryoinjury in zebrafish. *Development* **138**, 1663-1674.

González-Rosa, J. M., Peralta, M. and Mercader, N. (2012). Pan-epicardial lineage tracing reveals that epicardium derived cells give rise to myofibroblasts and perivascular cells during zebrafish heart regeneration. *Dev. Biol.* **370**, 173-186.

Han, P., Zhou, X.-H., Chang, N., Xiao, C.-L., Yan, S., Ren, H., Yang, X.-Z., Zhang, M.-L., Wu, Q., Tang, B. et al. (2014). Hydrogen peroxide primes heart regeneration with a derepression mechanism. *Cell Res.* **24**, 1091-1107.

Harrison, M. R. M., Bussmann, J., Huang, Y., Zhao, L., Osorio, A., Burns, C. G., Burns, C. E., Sucov, H. M., Siekmann, A. F. and Lien, C.-L. (2015). Chemokine-guided angiogenesis directs coronary vasculature formation in zebrafish. *Dev. Cell* **33**, 442-454.

Hauck, C. R., Hsia, D. A. and Schlaepfer, D. D. (2000). Focal adhesion kinase facilitates platelet-derived growth factor-BB-stimulated ERK2 activation required for chemotaxis migration of vascular smooth muscle cells. *J. Biol. Chem.* **275**, 41092-41099.

Hauck, C. R., Hsia, D. A. and Schlaepfer, D. D. (2002). The focal adhesion kinase–a regulator of cell migration and invasion. *IUBMB Life* **53**, 115-119.

Hu, N., Yost, H. J. and Clark, E. B. (2001). Cardiac morphology and blood pressure in the adult zebrafish. *Anat. Rec.* **264**, 1-12.

Humphries, J. D., Wang, P., Streuli, C., Geiger, B., Humphries, M. J. and Ballestrem, C. (2007). Vinculin controls focal adhesion formation by direct interactions with talin and actin. *J. Cell Biol.* **179**, 1043-1057.

Hwang, W. Y., Fu, Y., Reyon, D., Maeder, M. L., Tsai, S. Q., Sander, J. D., Peterson, R. T., Yeh, J.-R. J. and Joung, J. K. (2013). Efficient genome editing in zebrafish using a CRISPR-Cas system. *Nat. Biotechnol.* **31**, 227-229.

Ilić, D., Furuta, Y., Kanazawa, S., Takeda, N., Sobue, K., Nakatsuji, N., Nomura, S., Fujimoto, J., Okada, M. and Yamamoto, T. (1995). Reduced cell motility and enhanced focal adhesion contact formation in cells from FAK-deficient mice. *Nature* **377**, 539-544.

Kaelin, W. G., Jr. and Ratcliffe, P. J. (2008). Oxygen sensing by metazoans: the central role of the HIF hydroxylase pathway. *Mol. Cell* **30**, 393-402.

Kikuchi, K., Gupta, V., Wang, J., Holdway, J. E., Wills, A. A., Fang, Y. and Poss, K. D. (2011). tcf21+ epicardial cells adopt non-myocardial fates during zebrafish heart development and regeneration. *Development* **138**, 2895-2902.

Kim, J., Wu, Q., Zhang, Y., Wiens, K. M., Huang, Y., Rubin, N., Shimada, H., Handin, R. I., Chao, M. Y., Tuan, T.-L. et al. (2010). PDGF signaling is required for epicardial function and blood vessel formation in regenerating zebrafish hearts. *Proc. Natl. Acad. Sci. USA* **107**, 17206-17210.

Klemke, R. L., Cai, S., Giannini, A. L., Gallagher, P. J., de Lanerolle, P. and Cheresh, D. A. (1997). Regulation of cell motility by mitogen-activated protein kinase. *J. Cell Biol.* **137**, 481-492.

Koteliansky, V. E., Ogryzko, E. P., Zhidkova, N. I., Weller, P. A., Critchley, D. R., Vancompernolle, K., Vandekerckhove, J., Strasser, P., Way, M., Gimona, M. et al. (1992). An additional exon in the human vinculin gene specifically encodes meta-vinculin-specific difference peptide. Cross-species comparison reveals variable and conserved motifs in the meta-vinculin insert. *Eur. J. Biochem.* **205**, 1218.

Lepilina, A., Coon, A. N., Kikuchi, K., Holdway, J. E., Roberts, R. W., Burns, C. G. and Poss, K. D. (2006). A dynamic epicardial injury response supports progenitor cell activity during zebrafish heart regeneration. *Cell* **127**, 607-619.
Lifschitz-Mercer, B., Czernobilsky, B., Feldberg, E. and Geiger, B. (1997). Expression of the adherens junction protein vinculin in human basal and squamous cell tumors: relationship to invasiveness and metastatic potential. *Hum. Pathol.* **28**, 1230-1236.
Liu, Y.-G. and Chen, Y. (2007). High-efficiency thermal asymmetric interlaced PCR for amplification of unknown flanking sequences. *Biotechniques* **43**, 649-656, 652, 654 passim.
Liu, C., Ma, W., Su, W. and Zhang, J. (2012). Prdm14 acts upstream of islet2 transcription to regulate axon growth of primary motoneurons in zebrafish. *Development* **139**, 4591-4600.
Major, R. J. and Poss, K. D. (2007). Zebrafish heart regeneration as a model for cardiac tissue repair. *Drug Discov. Today Dis. Models* **4**, 219-225.
Manchenkov, T., Pasillas, M. P., Haddad, G. G. and Imam, F. B. (2015). Novel genes critical for hypoxic preconditioning in zebrafish are regulators of insulin and glucose metabolism. *G3* **5**, 1107-1116.
Missinato, M. A., Tobita, K., Romano, N., Carroll, J. A. and Tsang, M. (2015). Extracellular component hyaluronic acid and its receptor Hmmr are required for epicardial EMT during heart regeneration. *Cardiovasc. Res.* **107**, 487-498.
Mitra, S. K., Hanson, D. A. and Schlaepfer, D. D. (2005). Focal adhesion kinase: in command and control of cell motility. *Nat. Rev. Mol. Cell Biol.* **6**, 56-68.
Mitra, S. K., Mikolon, D., Molina, J. E., Hsia, D. A., Hanson, D. A., Chi, A., Lim, S.-T., Bernard-Trifilo, J. A., Ilic, D., Stupack, D. G. et al. (2006). Intrinsic FAK activity and Y925 phosphorylation facilitate an angiogenic switch in tumors. *Oncogene* **25**, 5969-5984.
Moiseyeva, E. P., Weller, P. A., Zhidkova, N. I., Corben, E. B., Patel, B., Jasinska, I., Koteliansky, V. E. and Critchley, D. R. (1993). Organization of the human gene encoding the cytoskeletal protein vinculin and the sequence of the vinculin promoter. *J. Biol. Chem.* **268**, 4318-4325.
Munoz-Chapuli, R., Gonzalez-Iriarte, M., Carmona, R., Atencia, G., Macias, D. and Perez-Pomares, J. M. (2002). Cellular precursors of the coronary arteries. *Tex. Heart Inst. J.* **29**, 243-249.
Olivey, H. E., Compton, L. A. and Barnett, J. V. (2004). Coronary vessel development: the epicardium delivers. *Trends Cardiovasc. Med.* **14**, 247-251.
Olson, T. M., Illenberger, S., Kishimoto, N. Y., Huttelmaier, S., Keating, M. T. and Jockusch, B. M. (2002). Metavinculin mutations alter actin interaction in dilated cardiomyopathy. *Circulation* **105**, 431-437.
Parsons, J. T. (2003). Focal adhesion kinase: the first ten years. *J. Cell Sci.* **116**, 1409-1416.
Pascoal, S., Esteves de Lima, J., Leslie, J. D., Hughes, S. M. and Saúde, L. (2013). Notch signalling is required for the formation of structurally stable muscle fibres in zebrafish. *PLoS ONE* **8**, e68021.
Peng, X., Ueda, H., Zhou, H., Stokol, T., Shen, T. L., Alcaraz, A., Nagy, T., Vassalli, J. D. and Guan, J. L. (2004). Overexpression of focal adhesion kinase in vascular endothelial cells promotes angiogenesis in transgenic mice. *Cardiovasc. Res.* **64**, 421-430.
Polte, T. R., Naftilan, A. J. and Hanks, S. K. (1994). Focal adhesion kinase is abundant in developing blood vessels and elevation of its phosphotyrosine content in vascular smooth muscle cells is a rapid response to angiotensin II. *J. Cell Biochem.* **55**, 106-119.
Poss, K. D., Wilson, L. G. and Keating, M. T. (2002). Heart regeneration in zebrafish. *Science* **298**, 2188-2190.
Raz, A. and Geiger, B. (1982). Altered organization of cell-substrate contacts and membrane-associated cytoskeleton in tumor cell variants exhibiting different metastatic capabilities. *Cancer Res.* **42**, 5183-5190.
Red-Horse, K., Ueno, H., Weissman, I. L. and Krasnow, M. A. (2010). Coronary arteries form by developmental reprogramming of venous cells. *Nature* **464**, 549-553.
Reese, D. E., Mikawa, T. and Bader, D. M. (2002). Development of the coronary vessel system. *Circ. Res.* **91**, 761-768.
Roman, B. L., Pham, V. N., Lawson, N. D., Kulik, M., Childs, S., Lekven, A. C., Garrity, D. M., Moon, R. T., Fishman, M. C., Lechleider, R. J. et al. (2002). Disruption of acvrl1 increases endothelial cell number in zebrafish cranial vessels. *Development* **129**, 3009-3019.
Seger, R. and Krebs, E. G. (1995). The MAPK signaling cascade. *FASEB J.* **9**, 726-735.
Shen, T.-L., Park, A. Y.-J., Alcaraz, A., Peng, X., Jang, I., Koni, P., Flavell, R. A., Gu, H. and Guan, J. L. (2005). Conditional knockout of focal adhesion kinase in endothelial cells reveals its role in angiogenesis and vascular development in late embryogenesis. *J. Cell Biol.* **169**, 941-952.
Simmons, D. G., Fortier, A. L. and Cross, J. C. (2007). Diverse subtypes and developmental origins of trophoblast giant cells in the mouse placenta. *Dev. Biol.* **304**, 567-578.
Staudt, D. and Stainier, D. (2012). Uncovering the molecular and cellular mechanisms of heart development using the zebrafish. *Annu. Rev. Genet.* **46**, 397-418.
Subauste, M. C., Pertz, O., Adamson, E. D., Turner, C. E., Junger, S. and Hahn, K. M. (2004). Vinculin modulation of paxillin–FAK interactions regulates ERK to control survival and motility. *J. Cell Biol.* **165**, 371-381.
Thisse, C. and Thisse, B. (2008). High-resolution in situ hybridization to whole-mount zebrafish embryos. *Nat. Protoc.* **3**, 59-69.
Turner, C. E. (2000). Paxillin and focal adhesion signalling. *Nat. Cell Biol.* **2**, E231-E236.
Vogel, B., Meder, B., Just, S., Laufer, C., Berger, I., Weber, S., Katus, H. A. and Rottbauer, W. (2009). *In-vivo* characterization of human dilated cardiomyopathy genes in zebrafish. *Biochem. Biophys. Res. Commun.* **390**, 516-522.
Vrancken Peeters, M.-P. F. M., Gittenberger-de Groot, A. C., Mentink, M. M. T. and Poelmann, R. E. (1999). Smooth muscle cells and fibroblasts of the coronary arteries derive from epithelial-mesenchymal transformation of the epicardium. *Anat. Embryol.* **199**, 367-378.
Westerfield, M. (2000). *The Zebrafish Book: A Guide for the Laboratory Use of Zebrafish (Danio rerio)*. Eugene, OR: University of Oregon Press.
Wilhelm, K., Happel, K., Eelen, G., Schoors, S., Oellerich, M. F., Lim, R., Zimmermann, B., Aspalter, I. M., Franco, C. A., Boettger, T. et al. (2016). FOXO1 couples metabolic activity and growth state in the vascular endothelium. *Nature* **529**, 216-220.
Wood, C. K., Turner, C. E., Jackson, P. and Critchley, D. R. (1994). Characterisation of the paxillin-binding site and the C-terminal focal adhesion targeting sequence in vinculin. *J. Cell Sci.* **107**, 709-717.
Wu, B., Zhang, Z., Lui, W., Chen, X., Wang, Y., Chamberlain, A. A., Moreno-Rodriguez, R. A., Markwald, R. R., O'Rourke, B. P., Sharp, D. J. et al. (2012). Endocardial cells form the coronary arteries by angiogenesis through myocardial-endocardial VEGF signaling. *Cell* **151**, 1083-1096.
Xu, W., Baribault, H. and Adamson, E. D. (1998a). Vinculin knockout results in heart and brain defects during embryonic development. *Development* **125**, 327-337.
Xu, W., Coll, J. L. and Adamson, E. D. (1998b). Rescue of the mutant phenotype by reexpression of full-length vinculin in null F9 cells; effects on cell locomotion by domain deleted vinculin. *J. Cell Sci.* **111**, 1535-1544.
Yang, J. and Xu, X. (2012). Immunostaining of dissected zebrafish embryonic heart. *J. Vis. Exp.*, e3510.
Zamir, E. and Geiger, B. (2001). Molecular complexity and dynamics of cell-matrix adhesions. *J. Cell Sci.* **114**, 3583-3590.
Zemljic-Harpf, A. E., Miller, J. C., Henderson, S. A., Wright, A. T., Manso, A. M., Elsherif, L., Dalton, N. D., Thor, A. K., Perkins, G. A., McCulloch, A. D. et al. (2007). Cardiac-myocyte-specific excision of the vinculin gene disrupts cellular junctions, causing sudden death or dilated cardiomyopathy. *Mol. Cell. Biol.* **27**, 7522-7537.
Zhao, X. and Guan, J.-L. (2011). Focal adhesion kinase and its signaling pathways in cell migration and angiogenesis. *Adv. Drug Deliv. Rev.* **63**, 610-615.
Ziegler, W. H., Liddington, R. C. and Critchley, D. R. (2006). The structure and regulation of vinculin. *Trends Cell Biol.* **16**, 453-460.